

Adaptive Quantized Planetary Crater Detection System for Autonomous Space Exploration

Aditri Paul*, Archan Paul†

*Manipal University Jaipur, India. Email: aditripaul@gmail.com

†Computational Scientist, India. Email: archanpaul@gmail.com

Abstract—Autonomous planetary exploration demands real-time, high-fidelity environmental perception. Standard deep learning models, however, require far more memory and compute than space-qualified, radiation-hardened, power-optimized hardware can provide. This limitation creates a severe design bottleneck. Engineers struggle to deploy sophisticated detection architectures without overloading the strict power and memory limits of onboard computers of outer space planetary exploration platforms.

In this foundational concept paper, we propose the Adaptive Quantized Planetary Crater Detection System (AQ-PCDSys) to resolve this bottleneck. We present an architectural blueprint integrating a Quantized Neural Network (QNN), refined through Quantization Aware Training (QAT), with an Adaptive Multi-Sensor Fusion (AMF) module and Multi-Scale Detection Heads. By forcing weights into low-precision integer arithmetic during the training and optimization phase, our framework strips away the floating-point overhead that typically overwhelms onboard computer’s processors. The AMF module directly addresses sensor fragility. It dynamically selects and fuses Optical Imagery (OI) and Digital Elevation Models (DEMs) at the feature level to provide reliable sensor inputs during extreme cross-illuminations and sudden sensor dropouts. As a concept paper, this work establishes the technical and mathematical justifications for the architecture rather than presenting completed empirical ablation studies. We outline a rigorous Hardware-in-the-Loop (HITL) evaluation protocol for immediate future validation, paving the way for next-generation, hardware-aware space-mission software.

Index Terms—Crater Detection, Deep Learning, Model Quantization, Attention Mechanisms, Computer Vision, Artificial Intelligence (AI), Real-Time Object Detection, Sensor Fusion, Edge AI.

I. INTRODUCTION

Autonomous planetary exploration hinges on a platform’s ability to recognize its surroundings in real-time. From the early Apollo landings to upcoming Artemis missions, real-time perception remains a prerequisite for mission’s success. Planetary craters are not merely topographical divots. They represent a fundamental geological record and function as fiducial markers for localization, terrain mapping, and hazard avoidance [2], [4]. Real-time crater detection solutions by the onboard platforms must therefore remain adaptive, resilient, and computationally lean. This capability enables precise navigation for landers and rovers operating autonomously without earth-based intervention.

Achieving this reliability in deep space introduces a severe contradiction. State-of-the-art deep learning models are highly capable but they require massive computational resources.

Conversely, space-qualified onboard hardware operates under brutal power, thermal, and memory constraints. This disparity between algorithmic demand and hardware capability exposes a primary bottleneck in current research.

Most single-modality detectors falter when confronted with extreme shadows or specular glare. Furthermore, standard full-precision implementations completely overwhelm the memory and computation power of typical onboard computers. While deep learning and sensor fusion are mature fields in terrestrial computing, their transition to space-qualified onboard hardware poses unique challenges. We frame this as a rigorous optimization problem: extracting high-density feature representations from high-bandwidth sensor streams without exceeding the finite throughput of space-grade onboard computers.

To bridge the gap between high-fidelity hybrid vision and radiation-hardened electronics, we introduce the Adaptive Quantized Planetary Crater Detection System (AQ-PCDSys) [10]. We present this manuscript as a foundational concept paper and architectural blueprint. Every design choice reflects the need for high-performance inference on processors with limited memory. Rather than attempting to compress heavy foundation models post-training, AQ-PCDSys operates as a ground-up, hardware-aware theoretical framework. Our sensor fusion logic is designed to be context-aware and hardware-optimized. It maximizes the extraction of salient data from Optical Imagery (OI) and Digital Elevation Models (DEMs) while strictly honoring hardware ceilings.

Because we scoped this work as a foundational concept paper, our immediate focus rests on establishing rigorous mathematical, structural and technical justifications. Explicit empirical benchmarking, detailed ablation studies, and final hardware telemetry remain deferred to our subsequent testing phase. The primary contributions of this paper are as follows:

- We present the architectural blueprint for a dual-backbone, QAT-native perception system specifically optimized for the rigid computational envelopes of radiation-hardened onboard space hardware.
- We mathematically formalize the Adaptive Multi-Sensor Fusion (AMF) module as a modality-specific spatial attention gate, providing theoretical robustness against spatial mis-registration and sensor dropout.
- We define a comprehensive Hardware-in-the-Loop (HITL) experimental protocol to empirically benchmark the system’s accuracy, latency, and power consumption

arXiv:2508.18025v3 [cs.LG] 4 Mar 2026

against existing baselines across extreme illumination scenarios.

II. RELATED WORK

The earliest efforts in planetary crater detection relied on classical image processing techniques like edge detection, morphological operations, and template matching [12], [13]. These tools provided a baseline, but their reliability is too limited for the unpredictable reality of space. A slight shift in solar angle or a patch of deep shadow strips these rule-based systems of their reliability. The physical variety of craters poses an equally frustrating challenge. Systems tuned for new, well-defined rims frequently fail upon encountering degraded or partially buried formations. This forces researchers into exhausting loops of manual re-calibration.

Convolutional Neural Networks (CNNs) introduced a vastly superior method for feature extraction. Remarkable accuracy can be achieved by using two-stage detectors, such as Faster R-CNN [11], by isolating potential regions of interest first. We found, however, that their heavy computational cost makes them entirely unsuitable for the real-time demands of an active automated-landing sequence. This realization pushed the research-community toward single-stage detectors like the YOLO series [6], [7]. Recent resource-efficient applications deploy YOLOv5 or YOLOv8 on commercial edge devices like the NVIDIA Jetson or Google Edge TPU. While these studies report concrete accuracy-latency trade-offs on martian/lunar datasets, they frequently document severe accuracy degradation under standard post-training quantization (PTQ). To mitigate quantization loss, Hardware-Aware Quantization (HAQ) and On-Chip Quantization (OHQ) frameworks automate mixed-precision bit-width assignments. There are some other established frameworks which advocate for 8-bit floating-point (FP8) precision to preserve dynamic range without the rounding errors of fixed-point math. We acknowledge the theoretical superiority of these advances. However, standard space-qualified flight computers and radiation-hardened FPGAs currently lack native FP8 arithmetic logic units. Consequently, AQ-PCDSys targets strict INT8 fixed-point execution to ensure immediate compatibility with available flight hardware.

Meanwhile, the computer vision community has shifted toward immense foundation models. Recent works explore Segment Anything Model (SAM)-based data-agnostic segmentation pipelines [16] and open-vocabulary detection frameworks [17]. These advanced architectures achieve impressive zero-shot generalization on lunar imagery. Yet, as highlighted in comprehensive crater-detection surveys [19], deployment of these systems on embedded hardware has not yet been available for full scale commercial use. Their reliance on heavy FP32 matrix operations fundamentally violates the strict thermal envelopes of flight-ready hardwares which are used in onboard computers of space exploration platforms. Finally, crater detection does not operate in isolation. It serves as the real-time perception front-end for broader localization systems. Architectures such as LunarNav [20] and ShadowNav

[21] demonstrate the absolute operational necessity of sensor-fusion for navigating extreme environments. Robust multi-modal designs, such as mixture-of-experts, utilize adaptive routing to maintain performance during sensor failures. We contextualize our own Adaptive Weighting Mechanism against these late-fusion precedents. AQ-PCDSys provides a computationally lighter alternative to MoME’s heavy routing networks by executing fusion at the feature level using simple, quantized spatial gating.

III. SYSTEM ARCHITECTURE AND METHODOLOGY

We developed the AQ-PCDSys framework to resolve the specific technical gaps identified in terrestrial perception models. The system operates as a unified architecture where each component strengthens the others. We conserve the computational capacity through quantization and deploy the spare computational power for the adaptive fusion module. We ensure the necessary balance between efficiency, stability, and accuracy using this tightly coupled design.

A. System Overview and Operational Context

We designed AQ-PCDSys to operate as an integrated perception module within a broader autonomous outer space navigation framework. Its primary mission is to resolve the bottleneck of executing intensive AI models on sparse, resource-constrained onboard computers.

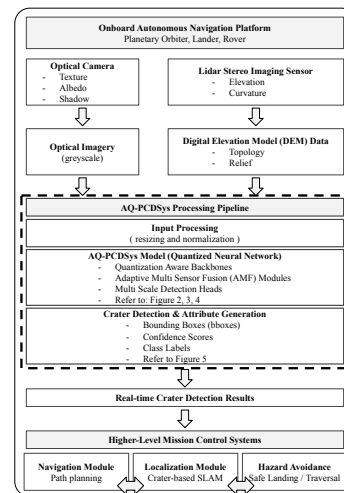


Fig. 1. High-level architecture of the autonomous navigation platform.

As depicted in Figure 1, the operational pipeline starts with Sensor Inputs. Onboard cameras capture grayscale imagery, yielding a sharp look at surface textures and albedo. This visual data, however, becomes unreliable in case of harsh illuminations and deceptive shadows. To bridge this gap, we simultaneously collect streaming data from LiDAR or stereo-imaging systems to build a Digital Elevation Model (DEM). This topographical information remains highly reliable as

DEM is generally immune to the shifting lighting conditions that confuses purely optical systems.

We route these continuous data streams directly to the Processing Pipeline of AQ-PCDSys. Once preprocessed, the core model executes the crater detection algorithms in real time. It distills the raw sensor influx into a live feed of actionable spatial attributes, specifically bounding boxes, confidence scores, and class labels. We directly feed this data as a stream to the Higher-Level Mission Control Systems in real-time. Supplying this direct feed to the Navigation, Localization, and Hazard Avoidance modules guarantees the autonomous platform possesses the split-second awareness required to survive a critical terminal descent during landing sequence of the space mission.

B. Overall Model Architecture

We built AQ-PCDSys around a novel Quantized Neural Network (illustrated in Figure 2), designed to function where the standard compute and memory intensive models fail due to the limitations of onboard computers. The primary driver of this performance is our integration of Quantization Aware Training (QAT). We didn't treat quantization as a retrospective compression/optimization step. Instead, we chose a training strategy that forces weights and activations to inhabit a low-precision space from the very first epoch. By compelling the network to learn within these tight numerical bounds, we shield detection accuracy from the unacceptable degradation that usually follows standard post-training compression.

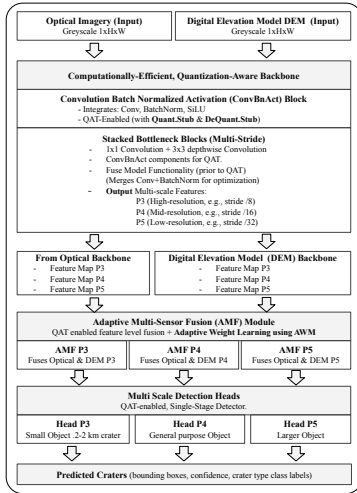


Fig. 2. Block diagram of the AQ-PCDSys Quantization-Aware Backbones, Adaptive Multi-Sensor Fusion module, and Multi-Scale Detection Heads.

A Quantization Aware Backbone (further discussed in next section) optimized for maximum efficiency is used at the core of this Quantized Neural Network. To bridge the gap between distinct data streams, we developed an Adaptive Multi-Sensor Fusion (AMF) module. Adaptive merging of the features from Optical Imagery (OI) and Digital Elevation Models (DEM)

provides the system with a highly decisive understanding of the terrain. We anchored this fusion in the Adaptive Weighting Mechanism (AWM). This mechanism enables the system to pivot between sensors (OI/DEM) based on the immediate planetary environment, prioritizing the more reliable modality whenever surface conditions compromise the other. Finally, specialized Multi-Scale Detection Heads process these fused features to predict craters across a vast range of sizes.

C. Computationally-Efficient, Quantization Aware Backbone

The backbone serves as the architecture's high-efficiency engine, utilizing depthwise separable Convolutions to maximize representational power while maintaining a low computational footprint. We constrain the model to a highly optimized profile of approximately 4.2 million parameters, requiring less than 2.0 GMACs for a standard 512×512 input resolution. This forward pass produces multi-scale feature tensors following standard pyramid scaling: $128 \times 64 \times 64$ (P3 scale at stride /8), $256 \times 32 \times 32$ (P4 scale at stride /16), and $512 \times 16 \times 16$ (P5 scale at stride /32).

Feature Level	Stride	Output Resolution	Channels
Input	—	512×512	3
P3 Scale	/8	64×64	128
P4 Scale	/16	32×32	256
P5 Scale	/32	16×16	512

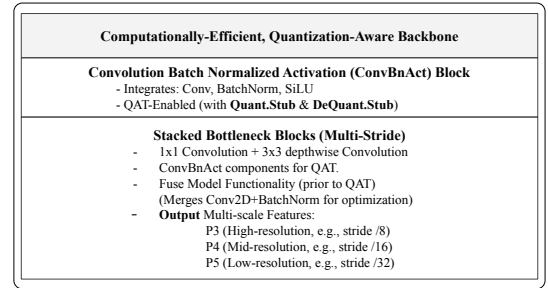


Fig. 3. Block diagram of Quantization Aware Backbone.

We designed the backbone specifically for Quantization Aware Training (QAT) [4], [8]. During the optimization phase the QAT simulates the constraints of lower numerical precision throughout the network. This forces the weights to adapt early, ensuring the model remains accurate upon deployment as a fully quantized entity. We anchor this adaptation in the simulation of quantization noise, mapping full-precision floating-point values (r) to lower-precision integers (q) through an affine mapping:

$$r \approx S(q - Z) \quad (1)$$

In this formulation, S represents a positive floating-point scale factor while Z acts as the integer zero-point. To ensure strict

compatibility with space-grade edge processors, we formalize this mapping through a mixed-granularity quantization scheme. We enforce symmetric per-channel quantization for the convolutional weights. This preserves the fine-grained statistical distribution of individual spatial filters without collapsing their dynamic ranges. To minimize memory bandwidth during matrix calculations, for the feature map activations we use asymmetric (affine) per-tensor quantization. This is further discussed in the section related to Adaptive Weighting Mechanism (AWM).

Handling non-linearities, such as the SiLU activation function and the Sigmoid gating within attention operations, require precise calibration. To avoid computationally expensive floating-point exponentials in resource constrained on-board computers, we pre-compute integer-based Look-Up Tables (LUTs) for these functions. We embed parameterized histogram-based observers into the network during the QAT loop. These observers track the statistical distribution of the activations, allowing the system to dynamically learn optimal clipping ranges and discard extreme outliers.

1) *Core Building Blocks of Backbone*: We structure the backbone around a streamlined Convolution-BatchNormalization-Activation (ConvBnAct) topology, engineered specifically to minimize memory bandwidth. We heavily substitute standard dense convolutions with depthwise separable convolutions. To prevent arithmetic overflow during high-dimensional mathematical operations on space-grade integer ALUs, we strictly enforce INT32 accumulators for all intermediate convolutional sums before downscaling the final activations back to INT8 bounds. This architectural choice factorizes the spatial and channel-wise feature extraction. Each convolutional layer is immediately followed by Batch Normalization (during training) and a SiLU non-linearity. To maintain strict INT8 compatibility during deployment, the SiLU activations are constrained by the dynamic clipping ranges learned via the histogram observers introduced in our QAT formulation.

2) *Fuse Model Functionality*: To maximize inference throughput on resource-constrained onboard computers, we structurally optimize the backbone before final deployment. In standard architectures, Batch Normalization (BN) requires isolated memory reads and mathematical scaling during inference. For AQ-PCDSys, we mathematically fold the BN parameters: γ (BN scale parameter), β (BN shift parameter), μ (BN mean), σ^2 (BN variance) directly into the preceding convolutional weights (W) and biases (b) along with ϵ , a small constant for numerical stability. The folded weights (W_{fold}) and biases (b_{fold}) are calculated as:

$$W_{fold} = \frac{\gamma}{\sqrt{\sigma^2 + \epsilon}} \cdot W \quad (2)$$

$$b_{fold} = \frac{\gamma}{\sqrt{\sigma^2 + \epsilon}} \cdot (b - \mu) + \beta \quad (3)$$

By executing this structural fusion, we eliminate Batch Normalization layers from the computational graph during

inference, reducing both computation and memory overheads. This fold is performed prior to the final INT8 quantization step; this ensures that the symmetric per-channel clipping ranges are calculated directly on the true, collapsed weight distribution. By doing so, we prevent compound truncation errors that typically occur when quantizing BN and Convolutional layers independently.

3) *Multi-Scale Feature Maps*: Planetary craters exhibit extreme scale variance, ranging from massive impact basins to localized, rover-scale hazards. To perceive these structures without the computational burden of processing an explicit image pyramid, the AQ-PCDSys backbone generates three parallel feature hierarchies from a single forward pass: P3 ($128 \times 64 \times 64$), P4 ($256 \times 32 \times 32$), and P5 ($512 \times 16 \times 16$).

The P3 tensor retains high-resolution spatial data critical for localizing dense, small-scale hazards. The P4 tensor encodes intermediate semantic density. It extracts the mid-resolution features necessary for general terrain mapping and mid-sized crater detection. Conversely, the heavily downsampled P5 tensor aggregates deep semantic context necessary for identifying massive, highly degraded crater rims. Rather than routing these tensors directly to standard detection heads, AQ-PCDSys feeds P3, P4, and P5 tensors from both the Optical and DEM backbones simultaneously to the Adaptive Multi-Sensor Fusion (AMF) module.

D. Adaptive Multi-Sensor Fusion (AMF) Module

We developed the AMF module to directly tackle the inherent fragility of single-modality sensing. In the unpredictable environments of planetary missions, relying on a single data source poses unacceptable operational risk. The module works across the parallel P3, P4, and P5 feature maps produced by our dual-backbone architecture. As shown in Figure 4, we consolidate this information at the feature level rather than the raw data stage. This ensures the network captures the nuanced interplay between visual textures and geometric heights.

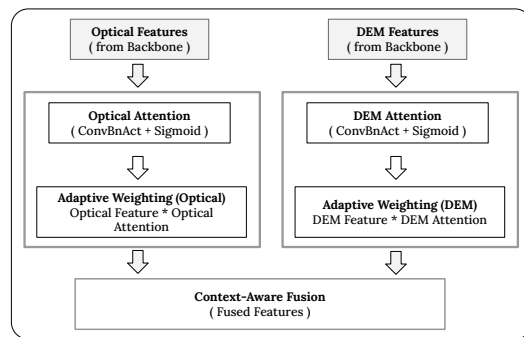


Fig. 4. Block diagram of the Adaptive Multi-Sensor Fusion (AMF) module.

The AMF module establishes deterministic sensor redundancy by co-processing Optical Imagery (OI) and Digital

Elevation Models (DEM) data streams. This architecture explicitly neutralizes the failure scenarios of isolated sensors. During terminal descent of landing sequence of space mission, deep shadows or solar glare frequently saturate optical sensors, causing catastrophic failure in standard camera-reliant models. The AMF module circumvents this hardware limitation. When optical telemetry degrades, the network mathematically suppresses the compromised feature channels. It shifts inference priority directly to the DEM data. Because DEMs measure absolute physical elevation independent of illumination, the system sustains continuous geometric tracking through complete optical blackouts. Simultaneously, the accuracy of the DEM data is augmented by OI data stream depending on the reliable availability.

1) *Parallel Feature Extraction*: We split the initial fusion process into two independent extraction branches which operate on QAT-optimized backbones. The Optical Feature branch extracts fine-grained textural details, albedo shifts, and complex shadow patterns. The DEM Feature branch handles the structural terrain geometry. It extracts elevation changes, slopes, and surface curvature to construct topographical cues completely independent of the sun’s position in the sky. Running these pipelines in parallel guarantees the system evaluates visual appearance and physical structure at the exact same time.

2) *Adaptive Weighting Mechanism (AWM)*: We centered the true intelligence of our OI and DEM data stream fusion strategy in the Adaptive Weighting Mechanism (AWM). Rather than relying on fixed logic for data stream integration/selection rules for feature level fusion, we formalized the AWM as a rigorous, modality-specific spatial attention gate. This component dynamically recalibrates the influence of each sensor stream in real-time based on learned illumination and topographical priors.

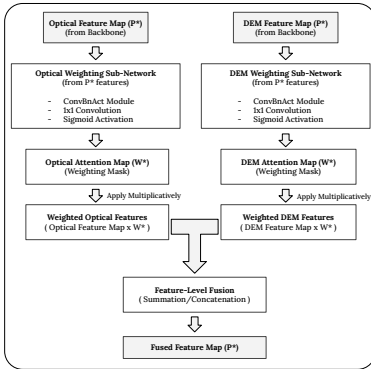


Fig. 5. Flowchart of Adaptive Weighting Mechanism (AWM).

The parallel processing of Optical and DEM backbones generate corresponding feature maps:

$$F_{OI} \in \mathbb{R}^{C \times H \times W} \quad (4)$$

$$F_{DEM} \in \mathbb{R}^{C \times H \times W} \quad (5)$$

The dimension C defines the total channel depth. The variables H and W set the spatial grid. The optical channels within F_{OI} encode strictly visual textures. They track contrast edges, localized shadows, albedo shifts, and specular glare. In parallel, the topographical channels within F_{DEM} map rigid structural geometry. They extract terrain gradients, slopes, and basin depths completely independent of planetary lighting conditions depending on the sun’s position in the sky. To evaluate these isolated features, we generate corresponding spatial attention maps, A_{OI} and A_{DEM} , using dedicated sub-networks:

$$A_{OI} = \sigma(\text{Conv}_{OI}(F_{OI})) \quad (6)$$

$$A_{DEM} = \sigma(\text{Conv}_{DEM}(F_{DEM})) \quad (7)$$

Here, Conv represents the attention sub-network (a ConvBnAct block followed by a 1×1 convolution), and σ is the sigmoid activation function scaling the spatial weights between 0 and 1. To prioritize the most reliable modality, the attention sub-networks function similar to established Convolutional Block Attention Modules (CBAM). Attention sub-networks help the system to learn and apply a learned weighting mask that emphasizes salient features while suppressing degraded features. In the event of blinding specular glare, the corresponding optical attention mask approaches zero and the network gracefully falls back onto the more reliable DEM stream.

Algorithm 1 Adaptive Weighting Mechanism (AWM)

Input: Optical Feature Map F_{OI} , DEM Feature Map F_{DEM}

Output: Fused Feature Map F_{Fused}

- 1: **Generate attention maps:**
 - 2: $A_{OI} \leftarrow \text{AttentionSubNetwork}_{OI}(F_{OI})$
 - 3: $A_{DEM} \leftarrow \text{AttentionSubNetwork}_{DEM}(F_{DEM})$
 - 4: **Apply weights via element-wise multiplication:**
 - 5: $F_{Weighted_OI} \leftarrow F_{OI} \odot A_{OI}$
 - 6: $F_{Weighted_DEM} \leftarrow F_{DEM} \odot A_{DEM}$
 - 7: **Fuse features:**
 - 8: $F_{Fused} \leftarrow \text{Concatenate}(F_{Weighted_OI}, F_{Weighted_DEM})$
 - 9: **return** F_{Fused}
-

Native INT8 execution of this multiplicative attention requires strict mathematical control to maintain fixed-point stability. While the raw inputs are 8-bit, the subtraction of learned zero-points ($q - Z$) necessitates a 9-bit signed representation. Consequently, the product of the feature map and attention map produces an intermediate value that can exceed 16-bit bounds. We utilize 32-bit integer (INT32) accumulators to handle these intermediate products and their subsequent summations without risk of numerical overflow. Immediately following this high-precision calculation, we apply a fixed-point requantization multiplier M to compress the 32-bit result back into the validated 8-bit output range:

$$M = \frac{S_F \cdot S_A}{S_{out}} \quad (8)$$

In this equation, S_F and S_A represent the floating-point scale factors for the feature and attention maps. The multiplier M serves as a pre-computed scaling bridge connecting these continuous floating-point spaces to the discrete integer logic of the hardware.

To execute the multiplicative attention (the multiplication of the feature map and the attention mask) on the actual hardware using discrete integer logic, the variables q_F and q_A represent the actual dynamic 8-bit integer values that M will ultimately rescale. The network tracks the mathematical baseline for these integers using learned zero-points, Z_F and Z_A . Multiplying these raw integers directly would produce mathematically meaningless results. Because affine quantization maps the true mathematical zero to an arbitrary 8-bit integer, multiplying unshifted values causes these artificial biases to compound and destroy the underlying feature data. To realign the integers with true zero, the hardware must first strip away the biases by subtracting the zero-points and the feature and attention values are multiplied as:

$$(q_F - Z_F) \cdot (q_A - Z_A) \quad (9)$$

using expanded 32-bit integer (INT32) accumulators as discussed previously to accommodate 18-bit output. By expanding into a 32-bit space, we guarantee the hardware absorbs the product without any risk of integer overflow. With the calculation complete, we apply the multiplier M to compress this intermediate INT32 result back down into our strict 8-bit bounds. To protect the integrity of the data during this aggressive downshift, we enforce nearest-even rounding and symmetric saturation clipping. The network dynamically calibrates the target output scale (S_{out}) using percentile observers during the initial QAT warm-up phase.

3) *Feature-Level Fusion and Channel Compression*: To finalize the AMF process, we merge the newly weighted signals into a single cohesive tensor. We integrate these refined streams strictly through concatenation along the channel dimension. Natively concatenating two independent INT8 streams, however, demands absolute scale alignment. Prior to stacking these tensors, we force a requantization step to align both $F_{Weighted_OI}$ and $F_{Weighted_DEM}$ to a shared output scale (S_{Fused}) and zero-point (Z_{Fused}).

The Optical and DEM branches each contribute a tensor with exactly C independent channels. Stacking them along the channel axis mathematically forces a combined tensor depth of $2C$. This expansion challenges the limited memory bandwidth of onboard computers. To mitigate these memory constraints, we immediately route the fused tensor through a lightweight 1×1 pointwise convolution. This operation compresses the channel dimensionality to C just prior to entering the detection heads. This final step guarantees we maintain our strict computational bounds.

4) *Justification Against Dynamic Alignment Constraints*: Recent advances in multi-modal fusion often rely on architectures like Deformable Convolutional Networks (DCN)

or Cross-Attention to mathematically compute pixel-by-pixel offsets and actively warp bounding boxes to force spatial alignment between mis-registered optical and LiDAR feeds. While these explicit alignment methods achieve state-of-the-art accuracy on datacenter hosted GPUs, we deliberately excluded them from AQ-PCDSys as our solution is designed for resource constrained onboard computers of space exploration missions. Also, the deformable alignment algorithms calculate dynamic, data-dependent spatial offsets for their convolution kernels. This degrades memory locality and triggers unpredictable cache misses, violating the strict deterministic execution bounds required by Real-Time Operating Systems (RTOS) used at onboard computer hardware. Similarly, Cross-Attention architectures require $O(N^2)$ for matrix operations and rely on Softmax, which are difficult to stabilize when approximated with INT8 hardware lookup tables (LUTs). Our choice of simple concatenation with independent per-modality spatial gating ensures strict $O(1)$ memory access predictability.

E. Multi-Scale Detection Heads

We implemented a set of Multi-Scale Detection Heads to act as the system’s final decision-makers. These specialized components take the high-level compressed feature maps and translate them into actionable detection results. We designed these heads as a single-stage, anchor-free detector. This architecture predicts crater attributes directly from center points, completely eliminating the dense, computationally heavy anchor-box generation required by multi-stage models.

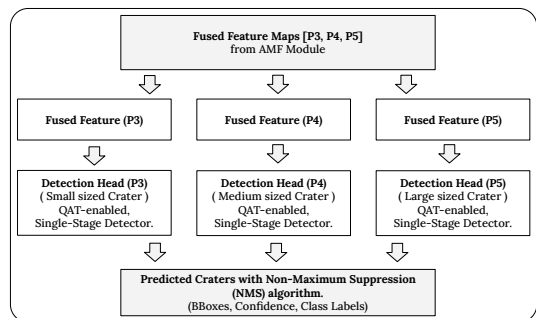


Fig. 6. Flowchart of the Multi-Scale Detection Heads.

1) *Hierarchical Object Prediction*: We built these heads to operate across the P3, P4, and P5 levels of the feature pyramid.

- Head P3 (stride /8): This head is designed to process detailed maps, optimized specifically to detect small craters (0.2–2.0 km wide). Small targets are the hardest to detect but the most dangerous during terminal descent of automated landing sequence of the space missions.
- Head P4 (stride /16): This head is designed for scanning mid-resolution feature maps to find mid-sized craters, acting as a reliable tool for general terrain mapping.

- Head P5 (stride /32): This head is used for the identification of massive craters and basins. These giant features serve as natural landmarks for absolute global localization.

By using an anchor-free detection strategy, we bypass rigid Intersection over Union (IoU) thresholding. Instead, we employ a dynamic label assignment mechanism. This strategy assigns ground-truth centers to the feature map locations with minimal classification and regression overhead. This dynamic center-sampling approach adapts seamlessly to the irregular morphology of degraded lunar craters.

F. Localization and Classification

We assign a dual workload to every detection head. The classification branch tackles the core identification problem by outputting a distinct confidence score for a given surface texture. The regression branch handles the physical geometry. It maps the exact spatial boundaries of the targeted crater. We define the final detection as:

$$\hat{B} = \{x_{\text{center}}, y_{\text{center}}, w, h, c\} \quad (10)$$

In this formulation, x_{center} and y_{center} pinpoint the exact spatial center of the crater, w and h establish the physical width and height of the bounding box, and c delivers the classification confidence score. Because we integrated these detection heads directly into our QAT loop, the network learns to calculate and output these physical bounding coordinates natively in INT8.

G. Post-Processing and Hazard Output

We focused the final task of our detection heads on organizing results into a clear hazard list. To resolve overlapping predictions, we execute Non-Maximum Suppression (NMS). Because NMS requires strict coordinate mathematics and IoU comparisons, we briefly dequantize the INT8 bounding box coordinates to FP16 just prior to the NMS algorithm. This hybrid execution prevents catastrophic integer-rounding degradation during final hazard resolution. The system then transmits these refined detections directly to the lander’s navigation computer, providing the autonomous platform with the instantaneous awareness required to avoid hazards.

IV. TRAINING METHODOLOGY AND DEPLOYMENT

Our training protocol is designed to simulate the challenges of planetary missions. We engineered the AQ-PCDSys learning phase to operate under extreme constraints from the very first epoch. We paired Quantization Aware Training (QAT) with highly variable, multi-sensor datasets. This deliberate pairing forces the network to execute feature extraction and fusion natively inside a low-precision mathematical space.

A. Data Sources and Environmental Augmentation

We ground our training process in high-resolution, scientifically validated datasets. We selected grayscale Optical Imagery (OI) from the Lunar Reconnaissance Orbiter Camera (LROC) Narrow Angle Camera (NAC). We carefully co-registered these images with Digital Elevation Model (DEM)

data, pulling 1.1m/px Digital Terrain Models (DTMs) from the South Pole-Aitken Basin. We sourced our ground truth annotations from the LU5M812TGT Lunar Crater Database.

To build true environmental resilience, we implemented a severe augmentation pipeline. We simulated solar illumination angles from 5° to 85° , creating a vast library of shadow patterns and illumination glare. Furthermore, we inject stochastic sensor-dropout augmentations during training. By intentionally zeroing out the optical or DEM tensors at random intervals, we force the network to rely on the surviving modality, mimicking the robust routing seen in Mixture-of-Experts models.

B. The Composite Loss Function

We force the network to learn accurate geometry and discard visual illusions by implementing a highly targeted Composite Loss Function. For each specific detection head (P_x), we calculate the total loss (L_{P_x}) as a weighted sum of three distinct components:

$$L_{P_x} = \lambda_{loc} \cdot L_{loc} + \lambda_{obj} \cdot L_{obj} + \lambda_{cls} \cdot L_{cls} \quad (11)$$

Where:

- L_{loc} calculates the physical bounding box error. We rely entirely on the Complete Intersection over Union (CIoU) metric to mathematically guarantee precise center-point alignment between the prediction and the true crater.
- L_{obj} calculates the objectness error using Binary Cross-Entropy (BCE). We intentionally split this out to teach the network the difference between actual physical geometry and misleading shadow patterns, effectively killing false positives at the root.
- L_{cls} provides the final classification verification, also using BCE, to confirm the detected object is actually a crater.

Backpropagating this complex loss through the QAT enabled network introduces a severe mathematical roadblock. Standard deep learning optimization requires smooth, continuous gradients. QAT, however, forces the weights through hard, non-differentiable integer rounding steps which may trigger vanishing gradient problem. To bypass this, we deploy a Straight-Through Estimator (STE). The STE mathematically tricks the optimizer during the backward pass, treating the harsh integer rounding as if it were a smooth, identity function. While this keeps the training loop alive, it introduces highly unstable, jagged gradient updates. To prevent these synthetic gradients from tearing the model apart, we implement a strict 5% linear warm-up schedule and clamp the updates using aggressive L2 gradient clipping to mitigate exploding gradient problem. By constraining the gradient norm $\|\mathbf{g}\|_2$ to a threshold $T = 1.0$, we mitigate the exploding gradient problem induced by the Straight-Through Estimator (STE) while preserving the directional integrity of the weight updates across the P3, P4, P5 feature scales.

$$\mathbf{g}_{clipped} = \begin{cases} \mathbf{g} & \text{if } \|\mathbf{g}\|_2 \leq T \\ T \frac{\mathbf{g}}{\|\mathbf{g}\|_2} & \text{if } \|\mathbf{g}\|_2 > T \end{cases} \quad (12)$$

C. The Small-Crater “Loss Boost”

Detecting small, shallow pits poses the greatest risk during final descent hazard avoidance. To prevent the network from focusing exclusively on massive impact basins, we introduced a strategic Loss Boost for the P3 detection head. We calculate the Total Loss (L_{total}) as:

$$L_{total} = (w_s \cdot L_{P3}) + L_{P4} + L_{P5} \quad (13)$$

Here, w_s functions as a Boost Hyperparameter, heavily amplifying errors made on fine-grained features. This forces the system to concentrate on the subtle hazards that matter most during terminal descent during landing sequence.

D. Optimization and Learning Rate Scheduler

We guide the training pace using an Adaptive Learning Rate Scheduler. We built this scheduler around a standard Exponential Decay model:

$$lr(e) = lr_0 \cdot \gamma^{(e/d)} \quad (14)$$

where:

- $lr(e)$ is the effective learning rate at epoch e .
- lr_0 is the initial learning rate magnitude;
- γ is the decay rate, the factor by which we control the learning pressure.
- d represents the decay interval, governing the frequency of the rate adjustment.

There is a need for a highly stable optimizer for the aggressive decay profile. We selected AdamW (which decouples the weight decay from the gradient update) specifically to meet this requirement and also establish rigid early-stopping bounds. Halting the training sequence at the first sign of plateauing completely prevents overfitting to the training distribution, guaranteeing the system learns the authentic planetary geology rather than localized statistical noise, by learning generalized morphological features.

E. Quantized Deployment

Upon completing QAT, we freeze the model into its fully quantized form, locking the parameters into memory-efficient 8-bit integers (INT8). We eliminated all floating-point dependencies to guarantee compatibility with the strict architectural constraints of radiation-hardened LEON/RAD processors and space-qualified ARM-class SoCs. Deploying these INT8 weights in deep space environments exposes the system to Single Event Upsets (SEUs), where high-energy particle strikes can induce bit-flips. Due to the reduced dynamic range of INT8, a single uncorrected flip in a weight tensor can catastrophically degrade detection accuracy. To secure the deployment of AQ-PCDSys, we mandate hardware-level Error Correction Codes (ECC) on the target SoC’s SRAM. At the software level, we pair the INT8 inference engine with Dual Modular Redundancy (DMR) and hardware watchdog timers, ensuring the module automatically restarts any calculation that violates deterministic timing bounds during critical descent operations.

V. SYSTEM ANALYSIS AND DISCUSSION

We evaluate the AQ-PCDSys architecture not as a collection of isolated algorithms, but as a unified, hardware-aware perception engine. The following subsections dissect this deliberate synergy. We first analyze how structural decisions mathematically bound our computational complexity. We then contextualize these savings against the brutal operational limits of computation hardware of deep space missions, specifically addressing the Edge AI challenges. Finally, we examine how the network inherently absorbs common failure modes like sensor dropout and spatial misalignment. We view the efficacy of AQ-PCDSys as the emergent outcome of deliberate synergy between its components.

A. Computational Complexity Analysis

We completely discarded standard 2D convolutions in favor of depthwise separable convolutions. A standard convolution demands heavy computational complexity:

$$\mathcal{O}(K^2 \cdot C_{in} \cdot C_{out} \cdot H \cdot W) \quad (15)$$

By factorizing the operation into a spatial depthwise convolution followed by a 1×1 pointwise projection, we reduce the total cost to:

$$\mathcal{O}((K^2 \cdot C_{in} \cdot H \cdot W) + (C_{in} \cdot C_{out} \cdot H \cdot W)) \quad (16)$$

where K represents the kernel size, C_{in} and C_{out} are the input and output channel depths, and H, W denote the feature map dimensions. This factorization achieves a theoretical complexity reduction of approximately $\frac{1}{C_{out}} + \frac{1}{K^2}$. When coupled with INT8 quantization, this architecture operates within the stringent power envelopes of space missions’ onboard computers without compromising the high-frequency sampling required for automatic navigation.

B. The Edge AI Challenges in a Space Context

We designed AQ-PCDSys to solve the “Edge AI Challenges” concerning accuracy, speed, and power use. In space, these trade-offs are unforgiving.

- **Power and Precision (INT8 vs FP8):** We strictly enforce INT8 quantization. This design choice directly targets the severe memory bandwidth limits of onboard systems. Recent terrestrial research heavily promotes 8-bit floating-point (FP8) precision to maintain dynamic range. We cannot adopt that standard here. Deep space flight hardware remains fundamentally legacy-driven. Standard radiation-hardened SoCs simply do not contain native FP8 arithmetic logic units. Our integer-based architecture therefore respects the physical constraints of the actual hardware.
- **DEM Overhead:** High-fidelity DEMs are not a readily available resource. A spacecraft has to synthesize these topographical maps live using active LiDAR or stereo photogrammetry. This upstream generation process consumes significant energy. Consequently, deploying the

AMF module forces mission planners to factor this specific sensor overhead directly into the total end-to-end power budget of the lander.

- **Latency:** Depthwise factorization forms the absolute core of our backbone. We have chosen this architecture to strictly bound the arithmetic complexity of matrix operations. We implemented a pure fixed-point execution pipeline to mitigate computational overhead, and allow the perception module to achieve the real-time processing speeds essential during automatic navigations.

C. Architectural Synergy and System Robustness

The AMF module directly mitigates two critical failure modes common in space missions:

- **Tolerance to Sensor Dropout:** Standard early-fusion networks experience catastrophic failure if one input channel corrupts. Conversely, our dual-backbone architecture processes OI and DEM streams independently. If the optical sensor suffers a temporary dropout, our Adaptive Weighting Mechanism dynamically drives the optical attention mask toward zero. The network seamlessly falls back onto the surviving topographical cues from the DEM data stream.
- **Robustness to Spatial Mis-registration:** Mechanical vibrations and telemetry delays frequently cause spatial mis-registration between OI and DEM streams. By delaying fusion until the higher semantic levels (P3, P4, and P5), AQ-PCDSys gains inherent spatial tolerance. A multi-pixel misalignment at the raw input resolution compresses into a negligible fraction of a pixel at the P5 feature scale. This deep structural synergy ensures that minor calibration offsets or parallax issues do not destroy the correlation between visual textures and underlying geometry.

VI. PROPOSED EXPERIMENTAL SETUP AND FUTURE EVALUATION PROTOCOL

As this manuscript serves as a foundational concept paper, the critical next phase of our research requires empirical validation. To transition AQ-PCDSys from theory to a mission-ready perception system, we designed a rigorous Hardware-in-the-Loop (HITL) evaluation protocol. This planned methodology explicitly measures resilience and benchmarks the hardware footprint.

A. Datasets and Cross-Illumination Partitions

Future evaluation will utilize the co-registered LROC NAC imagery and LOLA LiDAR DEM datasets. To systematically test sensor-fusion resilience, we will partition the test set into three distinct illumination regimes:

- **Midday/Standard Lighting (30° – 60°):** Baseline high-albedo contrast.
- **Extreme Cross-Illumination (5° – 15° and 75° – 85°):** Heavy shadow which distorts rim features.
- **Permanently Shadowed Regions (PSRs):** Zero optical utility, necessitating 100% DEM reliance.

Evaluation metrics will include standard Average Precision AP50 (Average Precision at IoU threshold = 0.50.), alongside AP30:60 (Average Precision across IoU thresholds from 0.30 to 0.60) specifically calibrated for the small crater bins (0.2–2.0 km diameter).

B. Testing with Hardware-in-the-Loop (HITL)

We do rigorous testing with Hardware-in-the-Loop (HITL) to bridge the gap between theoretical AI performance and the operational constraints of physical deployment. HITL evaluation is critical for spacebound systems as it exposes physical bottlenecks, such as memory bus contention, hardware-specific I/O latency, and thermal throttling, that software-based simulations often mask. We utilize the Apache TVM compiler stack to cross-compile the INT8 model for two representative aerospace testbeds: an NVIDIA Jetson Orin Nano (representing high-performance COTS systems) and a Microchip PolarFire SoC (representing radiation-tolerant, FPGA-based onboard hardware). By executing the architecture on target silicon, we extract empirical telemetry on Inference Latency (ms/frame), Peak Memory Utilization (tracking weights, activations, and transient buffers within SRAM), and Dynamic Power Consumption (W) under maximum computational load.

C. Baseline Architectures and Ablation Studies

We established our evaluation benchmarks to test AQ-PCDSys against both practical engineering alternatives and absolute theoretical ceilings. To prove our architecture actually delivers on its efficiency claims at the edge, we will pit it directly against INT8-quantized versions of YOLOv8-nano and MobileNet-SSD. These models serve as our primary operational baselines, representing the current standard for resource-constrained terrestrial detection. Simultaneously, we will execute our dataset against the Segment Anything Model (SAM). Deploying SAM on a spacecraft is computationally impossible, but evaluating it here provides a vital, uncompromising full-precision upper bound. This comparison definitively measures how much theoretical accuracy we sacrifice to fit within the strict physical bounds of flight hardware.

To further isolate the efficacy of our internal architectural choices, future work will evaluate a comprehensive set of ablation studies:

- **Modality and Dropout Ablation:** We will benchmark the fully fused AQ-PCDSys against single-modality variants. We will inject synthetic sensor dropout to definitively prove the spatial attention gate’s ability to degrade gracefully.
- **Quantization Paradigm:** We will compare the target INT8 QAT model against a full-precision FP32 baseline and a standard Post Training Quantization (PTQ) model.
- **Mixed-Precision Exploration:** We intend to adopt Hardware-Aware Quantization (HAQ) in our upcoming builds. This framework automates mixed-precision routing by dynamically mapping 4-bit and 8-bit assignments across the network layers. Handing this optimization step

over to an HAQ controller guarantees a much steeper drop in inference latency.

VII. CONCLUSION AND FUTURE DIRECTIONS

The strict power, memory, and thermal limits of radiation-hardened hardware severely restrict the deployment of advanced deep learning models in onboard hardware of autonomous deepspace missions. We engineered the Adaptive Quantized Planetary Crater Detection System (AQ-PCDSys) to resolve this bottleneck. Our hardware-aware architecture bridges the massive gap between terrestrial computer vision algorithms and the challenges of extraterrestrial operations. We embedded Quantization Aware Training (QAT) directly into the network backbone. This structural choice mitigates the floating-point overhead. The system relies entirely on INT8 arithmetic to sustain high throughput within extreme SRAM limits. Simultaneously, the Adaptive Multi-Sensor Fusion (AMF) module mitigates the inherent fragility of single-modality sensors. The network dynamically gates and compresses optical and topographical features. This fusion mechanism absorbs telemetry time-skew and defaults to reliable DEM geometries the moment optical sensors fail.

Beyond standalone inference, this architectural blueprint lays the groundwork for distributed intelligent computing. Our quantization framework directly supports onboard continual calibration. Deep space radiation inevitably degrades optical sensors over time. When this occurs, the space missions' computers can autonomously mitigate the situation. Upcoming lunar missions will also depend on multi-agent robotic swarms. The Deep Space Network cannot handle the massive bandwidth required to transmit raw optical data home for retraining. AQ-PCDSys solves this challenge using smart edge AI integrations. Decentralized landers extract localized gradient updates from their unique terrain encounters. The swarms then share these highly compressed, integer-based updates across low-bandwidth Inter-Satellite Links. This capability proves the immediate viability of autonomous federated learning on other planets.

We have established the structural and mathematical foundation for this architecture. Our immediate next phase targets empirical validation. We will execute the rigorous Hardware-in-the-Loop (HITL) evaluation protocol on proxy spaceflight processors. Validating these integer-based models on actual edge hardware will confirm our theoretical benchmarks. We intend to demonstrate that AQ-PCDSys delivers the real-time, high-fidelity perception necessary to guarantee safe, autonomous planetary landings.

REFERENCES

- [1] Fassett, C., et al. "Lunar impact basins: Stratigraphy, sequence and ages from superposed crater populations measured from Lunar Orbiter Laser Altimeter (LOLA) data." *J. Geophys. Res. Planets* 117.E12 (2012).
- [2] Head, J. W., et al. "Global distribution of large lunar craters: Implications for resurfacing and impactor populations." *Science* 329.5998 (2010): 1504-1507.
- [3] He, K., et al. "Mask R-CNN." *Proceedings of the IEEE international conference on computer vision* (2017): 2961-269.
- [4] Jacob, B., et al. "Quantization and training of neural networks for efficient integer-arithmetic-only inference." *Proceedings of the IEEE conference on computer vision and pattern recognition* (2018): 2704-2713.
- [5] Jia, Y., Liu, L., Zhang, C. "Moon crater detection using nested attention mechanism based UNet++." *IEEE Access* 9 (2021): 44107-44116.
- [6] Jocher, G., et al. "ultralytics/yolov5: v3.1 - Bug Fixes and Performance Improvements." *Zenodo* (2020).
- [7] Joseph, R., et al. "You Only Look Once: Unified, Real-Time Object Detection." *Proceedings of the IEEE conference on computer vision and pattern recognition* (2016): 779-788.
- [8] Krishnamoorthi, R. "Quantizing deep convolutional networks for efficient inference: A survey." *arXiv preprint arXiv:1806.08342* (2018).
- [9] Lin, X., et al. "Lunar Crater Detection on Digital Elevation Model: A Complete Workflow Using Deep Learning and Its Application." *Remote Sensing* 14.3 (2022): 621.
- [10] Paul, A., et al. "AQ-PCDSys: Adaptive Quantized Planetary Crater Detection System for Autonomous Outer Space Planetary Exploration." (2025), Patent Pending.
- [11] Ren, S., et al. "Faster R-CNN: Towards Real-Time Object Detection with Region Proposal Networks." *Advances in neural information processing systems* 28 (2015).
- [12] Salamunićar, G., & Lončarić, S. "Manual feature extraction in lunar studies." *Computers & Geosciences* 34.10 (2008): 1217-1228.
- [13] Zuo, W., et al. "Contour-based automatic crater recognition using digital elevation models from Chang'E missions." *Computers & Geosciences* 97 (2016): 79-88.
- [14] Vaswani, A., et al. "Attention is all you need." *Advances in neural information processing systems* 30 (2017).
- [15] Li, S., et al. "Autonomous planetary crater detection via Quantization Aware pyramid networks." *ISPRS journal of photogrammetry and remote sensing* 220 (2025).
- [16] Giannakis, I., et al. "Deep learning universal crater detection using Segment Anything Model (SAM)." *arXiv preprint arXiv:2304.07764* (2023).
- [17] Bauer, P., et al. "Vision-Language Model for Accurate Crater Detection." *arXiv preprint arXiv:2601.07795* (2026).
- [18] Song, J., et al. "Explainable Convolutional Networks for Crater Detection and Lunar Landing Navigation." *arXiv preprint arXiv:2408.13587* (2024).
- [19] Tewari, A., et al. "Deep Learning based Systems for Crater Detection: A Review." *arXiv preprint arXiv: 2310.07727* (2023).
- [20] Daftry, S., et al. "LunarNav: Crater-based Localization for Long-range Autonomous Lunar Rover Navigation." *arXiv preprint arXiv:2301.01350* (2023).
- [21] Atha, D., et al. "ShadowNav: Autonomous Global Localization for Lunar Navigation in Darkness." *arXiv preprint arXiv:2405.01673* (2024).